# SAR Data Focusing Using Seismic Migration Techniques

C. CAFFORIO
C. PRATI
F. ROCCA
Politecnico di Milano

**Conventional algorithms for synthetic aperture radar (SAR) data focusing use the matched filter concept and convolve the data with a reference phase signal which changes with range. The resulting algorithm is space variant and its frequency domain implementation is cumbersome.**

**SAR data, however, can be focused using migration techniques, quite similar to those used in geophysics. The frequency-wavenumber approach is extremely efficient: it attains almost the ultimate results in performance, with the efficiency of frequency domain implementation. The method is exact when the sensor flies along a rectilinear path, but even with a spherical Earth and a circular sensor trajectory the results are extremely good. Terrestrial swaths as wide as 100 km can be focused simultaneously with no serious degradation, at least with the spatial resolution at present used or envisaged in SAR missions.**

**The algorithm has been tested with synthetic data, with SEASAT-A data and with airplane data (NASA-AIR). The experimental results fully support the theoretical analysis.**

Manuscript received June 20, 1988; revised July 10, 1989 and February 14, 1990.

IEEE Log No. 41898.

This work was supported by the European Space Agency under Contract 7998/88/F/FL(SC).

Authors' current addresses: C. Cafforio, Dipartimento di Elettrotecnica ed Elettronica, University of Bari, Italy; C. Prati, Centro Studi Telecommunicazioni Spaziali, National Research Council, Milan, Italy; F. Rocca, Dipartimento di Elettronica, Politecnio di Milano, Piazza L. da Vinci, 32-20133, Milano, Italy.

0018-9251/91/0300-0194 $1.00 © 1991 IEEE

## I. INTRODUCTION

The remote sensing of resources of the Earth can be carried out using electromagnetic waves at optical frequencies and microwaves in the 3–30 cm wavelength range [1]. The spatial resolution of the survey is dependent upon the bandwidth of the source, upon the width of the beams of the receiver and transmitter antennae, and upon the distance between the observation platform and the surface. The platform can be placed on an airplane or on a satellite [2–5]. For reasons of continuous availability, satellites are preferable.

Despite the very large distance entailed by a satellite borne sensor, it is still possible to achieve a satisfying spatial resolution using synthetic aperture radar (SAR) techniques. These methods are shown to be substantially identical to the techniques used for seismic surveying [6–8], though SAR uses different waves. The resolution achieved in the published experiments is on the order of 20 m from 800 km.

This high resolution is obtained if the scattered wavefield is processed so that a wide receiving antenna is simulated. This corresponds to an extremely narrow antenna beam. In the case of SAR data, the processing has been carried out optically first, then using digital techniques, but adopting algorithms that require unnecessary approximations, or being overloaded by unnecessarily lengthy calculations, as it is shown in detail in Section IID.

In effect, it is easy to show that there are no differences with respect to seismic migration for bandpass data, both in the temporal as well as in the spatial domain. Thus, the same revolution experienced in seismics with the introduction of wave equation migration [8] is now possible in radar, with all the consequent advantages in processing precision and in decreased costs.

The applications of SAR sensing are very relevant to all kinds of remote sensing since radiation penetrates clouds and foliage. If the terrain is arid, radiation penetrates the upper layers of the terrain and reaches either the water level or the rocks buried below [10] that reflect microwaves.

Since penetration increases with wavelength, it is interesting to work toward lower frequencies. However, this approach has prohibitive computing costs if the classical techniques are used. With the introduction of wave equation, the cost of the processing is virtually independent of the surveying wavelength. New opportunities are thus found for an increased use of this type of surveys in a wide range of applications.

### A. SAR Basics

The theory of SAR systems has been worked out in detail elsewhere, so the preliminaries will be kept at a

minimum; just the basics will be presented to make the paper self-consistent.

The SAR system is a conventional pulsed radar which takes advantage of the relative motion between sensor and target to synthesize a very long antenna and to achieve a high cross-range resolution. How range resolution is obtained is not relevant; as long as the SAR principle is concerned, it can likewise be obtained through extremely short transmitted pulses, or with longer coded (e.g., linearly frequency modulated or "chirp") pulses that, after reception, are compressed into shorter waveforms. What is basic is that each echo retains both its amplitude and its phase. It is usual to adopt the complex envelope representation in which the received signal is complex, with its real and imaginary parts obtained through quadrature demodulation [3] from the incoming bandpass signal.

Notice that from here on we indicate with the angular frequency ($\omega$) the variable conjugate to the arrival time ($t$) and with the wavenumber ($k_x$) the variable conjugate to the along track space variable ($x$). In the future, we also indicate the across-track spatial coordinate with ($z$), and its conjugate variable as ($k_z$). The key of the method is in the change of variable from ($\omega$) to ($k_z$), that we call Stolt interpolation [7].

Let us consider the radar sensor flying over the back-scattering Earth as shown in Fig. 1. A single scatterer, as long as it stays within the antenna footprint, produces a series of echoes with arrival times and phase delays that are functions of the sensor position with respect to the elementary scatterer. In SAR, the relative motion between sensor and target is supposed known. Conventional focusing algorithms estimate the back scattering coefficient of an elementary cell by picking up from the received data the samples with the right sequence of time delays and correlating them with the corresponding sequence of phase delays [2, 3]. The change from scan to scan in the echo time delay is known as "range migration", while the sequence of phase delays of the echoes coming from a single scatterer is the "target Doppler history".

An implementation of the focusing algorithm in the time (range)–space (azimuth) domain can get the ultimate resolution out of the received data, but at the cost of a very poor computational efficiency. Other, more efficient techniques, based on the polyphase algorithm have been recently proposed by the authors [11]. Other algorithms [3] take into account only the linear and the quadratic terms of range migration (respectively "range walk" and "range curvature") and approximate the phase history $r(x)$ of the point target with a linear frequency modulated signal. Obviously, the resolution of the focused image is poorer.

Time-wavenumber domain implementations are particularly appealing, due to the efficiency of fast Fourier transform (FFT); up to now, they

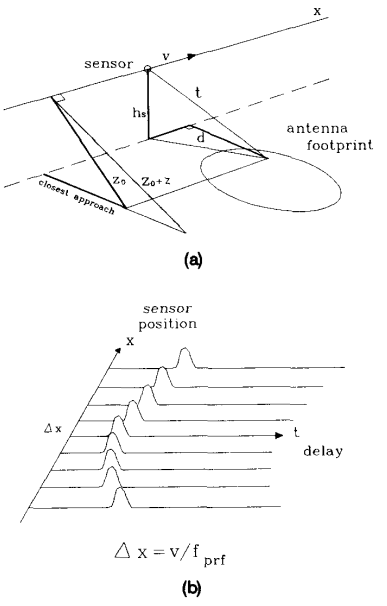


Fig. 1. SAR system geometry. (a) Echoes from a point scatterer. (b) Envelopes of RF returns.

have suffered the limitations due to an approximate range migration correction and to the necessity of accommodating the variations of the Doppler signature with range by a segmentation of the range swath into shorter segments [3].

The algorithm presented here works in the $\omega - k_x$ domain and therefore time delays can be easily accommodated with phase shifts that increase linearly with $\omega$. Thus range migration poses no problem at all.

Framing the SAR focusing problem into the framework of wavefield migration, an algorithm can be derived that overcomes most of the aforesaid problems. This algorithm is known to geophysicists as the $\omega - k$ *migration method*, even though a few modifications are necessary to adapt it to the new problem [6, 7]. A good tutorial can be found in [8].

Section II describes the algorithm in plane geometry first, where range migration and phase history can be exactly matched. The effects of the sphericity of the Earth, of the earth rotation, and of the satellite trajectory curvature are taken into account in Section III, showing that the theoretically achievable spatial resolution is well within the requirements of present day and near future SAR missions.

## II. $\Omega - K$ MIGRATION IN PLANE GEOMETRY

### A. Radiating Reflector Model

The electromagnetic pulse, radiated from the antenna, impinges on the ground and is scattered back toward the radar antenna. The reflected field

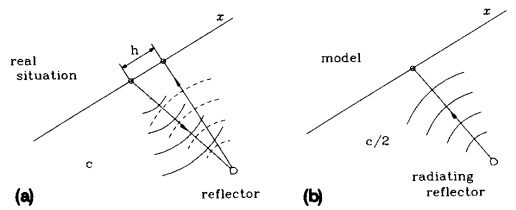


Fig. 2. (a) Real SAR situation. (b) The "radiating reflectors" model.

can, however, be thought to originate from the scatterers and to propagate towards the antenna. The contributions from different point scatterers should arrive at different times, with delays proportional to their distances from the antenna. If all elementary scatterers radiate simultaneously and the propagation velocity in the medium is supposed to be one half of the true value, the kinematics of the actual wavefield are well reproduced. This is the exploding reflectors model used in geophysics [7] and in this context the $\omega - k$ focusing technique is easily understood. The solution to the inverse problem which is obtained using this model produces an estimate of the field radiated back by the reflecting bodies; small corrections are required to determine thereafter the reflection coefficients.

There are differences between the model and the real situation (Fig. 2), and it is useful to state them clearly. First of all, notice that the sensor motion during the pulse time of flight has been neglected. In other words we have supposed that the satellite moves in a "stop and go" manner. In this ideal situation, transmission and reception of the chirp are performed during the halting period. This is obviously in contrast with the real situation since 1) the platform transmits and receives the radio frequency chirp at different orbit positions (the sensor travels a short distance $h$ during the pulse traveltime), and 2) the platform moves during the transmission and the reception of RF chirp and the Doppler effect changes the linear frequency modulation of the reflected signal (train whistle effect).

A complete mathematical description of this effect can be found in [9]. For satellite geometry, however, this effect can be neglected because of the large bandwidth of the radar. Furthermore, if we consider just the traveltimes, in all practical cases the offset $h$ (42 m in the case of SEASAT) between transmitter and receiver can be neglected, since the sensor velocity $v$ is small compared with the propagation velocity that, for radar, is the velocity of light $c$. In the SEASAT case, as an example, the length of the effective ray path is 0.235 mm longer than that computed with the radiating reflector model. Thus, the traveltimes (phases) of the radiating reflector model can be taken as correct. Passing to amplitudes, the backscattered wavefield is proportional to

$$\frac{\exp(-j4\pi R/\lambda)}{R^2} \tag{1}$$

where $R$ is the sensor-target distance and $\lambda$ is the radiation wavelength.

However, the amplitude in the model is different, being proportional to $1/R$ due to the one way propagation path, while in the real case it is proportional to $1/R^2$. Nonetheless, the largest sensor-receiver distance variation during the interval of observation (for the SEASAT case) is about 58 m that must be compared with the closest approach distance of about 850Km. Thus, the amplitude variation due to the $1/R^2$ term (the real situation) is 0.999863 whereas that due to the term $1/R$ (the model) is 0.99993. The difference can be neglected with respect to the antenna pattern. Obviously, there is still a range varying gain to be compensated as usual.

## B. Focusing Through Wave Migration

Accepting the radiating reflector model, it is possible to consider the operation of the pulsed radar in motion as the sampling of the radiated (in effects, backscattered) field on a set of points along the sensor trajectory. The geometry of the system is again that of Fig. 1. The sampling distance $\Delta x$ depends on the satellite velocity $v$, and on the constant transmitter pulse repetition frequency $f_{\text{prf}}$:

$$\Delta x = \frac{v}{f_{\text{prf}}}. \tag{2}$$

The problem is linear and, therefore, the superposition principle applies and we can consider a single point source. If the sampling is along a straight line, the problem has a cylindrical symmetry. Whichever the source position around the line of sensors, the measured field strengths will always be the same, as long as the source is located at the same distance from and at the same position along the line. All sources can be thought to lie on a conceptual plane that contains the sensor trajectory, with no loss of generality. Henceforth $x$ will identify the position along the line of sensors and $z$ the distance in that conceptual plane in the direction orthogonal to $x$. The coordinate along the crossing spatial axis will be denominated $y$.

A point source radiates, at time $t = 0$, a spherical wave that reaches the sampling points after different time intervals. If the source is placed in $(x_0, z_0)$ the time $t(x, x_0, z_0)$ at which the wavefront arrives at the sampling point in $x$ is

$$t(x, x_0, z_0) = \frac{2}{c}\sqrt{(x - x_0)^2 + z_0^2}. \tag{3}$$

(This is the Doppler history).

The arrival times relative to the same source (echoes relative to the same scatterer), if displayed in the $x-t$ plane (see Fig. 1(b)), cluster along a curve which is a hyperbola with apex in $x_0$ (the along track position of the point source), $t_0 = 2z_0/c$. The field due to a distribution $s(x,z)$ of sources emitting at time $t = 0$, as measured along the sensor path, can be expressed in terms of time delays (3):

$$\Psi(x, y = 0, z = 0, \omega) = \frac{1}{4\pi} \iiint s(x', z') \cdot \delta(y') \cdot \frac{e^{-j(2\omega/c)\sqrt{(x-x')^2+y'^2+z'^2}}}{\sqrt{(x-x')^2+y'^2+z'^2}} \cdot dx'\, dy'\, dz' = \frac{1}{4\pi} \iint s(x', z') \cdot \frac{e^{-j\omega t(x,x',z')}}{R} \cdot dx'\, dz'. \quad (4)$$

The information on the amplitude and location of the point source, is distributed along this hyperbolic curve. Now, if $z_0$ was zero, i.e., with a hypothetical sensor flying at ground level over the scatterer, the received wavefield would contain, at time $t = 0$, a spike in $x_0$ with an amplitude proportional to the reflectivity of the scatterer. Therefore, one way to invert (4) is to "downward continue" the wavefield along the $z$ axis, and then to determine the amplitudes of the wavefield, after downward continuation, at time $t = 0$ at the sources location.

Downward continuation here stands for the operation with which the wavefield at level $z_0$ can be computed, given the wavefield at level $z$. Downward continuation can be easily carried out by decomposing the received wavefront in a sum of planar waves, downward continuing each of them separately, and then recombining them at the proper time. This sequence of operations can be efficiently performed in the frequency-wavenumber domain.

### C. Focusing in Frequency-Wave Number Domain

Let the complex function $d(x, z = 0, t)$ represent the received data, after the proper compression of the transmitted pulse waveform. It can be expressed as a weighted sum of complex exponentials:

$$d(x, z = 0, t) = \frac{1}{(2\pi)^2} \iint D(k_x, z = 0, \omega) \cdot e^{j(\omega t + k_x x)}\, d\omega\, dk_x \quad (5)$$

where $D(k_x, z = 0, \omega)$ is the two-dimensional Fourier transform of the data:

$$D(k_x, z = 0, \omega) = \iint d(x, z = 0, t) \cdot e^{-j(\omega t + k_x x)}\, dx\, dt. \quad (6)$$

Any scalar monochromatic plane wave, with wavefront orthogonal to the $x - z$ plane, can be described by the expression $D(k_x,\omega)\exp[j(\omega t + k_x x + k_z z)]$. The measured field values can, therefore, be considered to be the result of the superposition of plane waves with different wavelengths and wavenumbers, whose amplitudes are expressed, for $z = 0$ and as a function of $\omega$ and $k_x$, by $D(k_x, z = 0, \omega)$.

A proper backpropagation of the measured field can bring back the source values. Once the field has been decomposed into monochromatic plane waves, its downward continuation consists simply in the application of the proper phase rotation to each plane wave.

As is well known, wavelength $\lambda$ and wavenumbers $k_x$ and $k_z$ ($k_y$ is supposedly zero) are linked together by

$$\lambda = \frac{\pi c}{\omega}; \qquad k_x = \frac{2\pi}{\lambda}\sin\theta; \qquad k_z = \frac{2\pi}{\lambda}\cos\theta \quad (7)$$

so that

$$\omega = \frac{c}{2} \cdot \sqrt{k_x^2 + k_z^2}. \quad (8)$$

The angle $\theta$ is the angle of incidence of the radiation. The phase delay due to propagation over a distance $R$ is $2\pi R/\lambda$. The phase operator required to back propagate, from $z = 0$ to $z = z_0$, a plane wave with given $\omega$ and $k_x$ is $e^{j\varphi}$, where:

$$\varphi = k_z z_0 = \frac{2\omega}{c}\sqrt{1 - \frac{k_x^2 c^2}{4\omega^2}} \cdot z_0. \quad (9)$$

The wavefield at depth $z$ can, therefore, be expressed, in the $\omega - k_x$ domain, as

$$D(k_x, z, \omega) = D(k_x, z = 0, \omega)e^{jk_z z}. \quad (10)$$

A much faster way to obtain (10) is to exploit directly the two-dimensional wave equation:

$$\frac{\partial^2 D}{\partial x^2} + \frac{\partial^2 D}{\partial z^2} = \frac{\partial^2 D}{\partial t^2}\frac{1}{c^2}. \quad (11)$$

Equation (10) provides a solution of the wave equation after Fourier transform along spatial and temporal axes and use of the separation equation (8). The wave equation (11) applies to seismic as well as SAR. We chose the other way in order not to bypass the intrinsic spatial 3-dimensionality of the problem as further analyzed in the appendix. We have to handle point sources in 3-D space and not line sources as implied by (11).

Since in this section the origin of time is placed when the collection of data starts, the measured field is considered to be produced by sources exploding at a time $t = -t_0$. A map of the "sources" can then be obtained by propagating the wavefield at depth $z$ backward in time by an amount $t_0$, i.e., by computing

$d(x,z,t=-t_0)$:

$$d(x,z,t=-t_0) = \frac{1}{(2\pi)^2}\int_{-\omega_0-\omega_s/2}^{\omega_0+\omega_s/2} d\omega \int_{k_{x\min}}^{k_{x\max}} D(k_x,z=0,\omega) \cdot e^{jk_x z} e^{j[k_x x+\omega(-t_0)]}\, dk_x. \quad (12)$$

Formula (12) gives the focusing and can be modified to improve the computational efficiency. It can be noted that the $\omega$ variable (the data frequency) ranges between $-\omega_0-\omega_s/2$ and $\omega_0+\omega_s/2$, where $\omega_0$ represents the radar carrier frequency (in the order of 1 GHz for practical applications) and $\omega_s$ represents the transmitted signal bandwidth (tens of MHz). Since SAR signals are narrowband and their spectrum is originally centered around the radar carrier frequency $\omega_0$ there is no reason to integrate on a wide band (i.e., the spectrum is symmetric and the integral between $-\omega_0+\omega_s/2$ and $\omega_0-\omega_s/2$ is null). In fact it is easy to realize that the same result of formula (12) can be achieved by limiting the above said integral between $-\omega_s/2$ and $+\omega_s/2$ provided that the variable $\omega$, inside the integral, is changed into $\omega'+\omega_0$.

Thus, the following equation holds

$$d(x,z,t=-t_0) = \frac{1}{(2\pi)^2}\int_{-\omega_s/2}^{+\omega_s/2} d\omega' \int_{k_{x\min}}^{k_{x\max}} D'(k_x,z=0,\omega') \cdot e^{jk_x z} e^{j[k_x x+(\omega'+\omega_0)(-t_0)]}\, dk_x \quad (13)$$

where $D'(k_x,z=0,\omega')$ represents the Fourier transform of the data after frequency shift.

$$D'(k_x,z=0,\omega') = 2\cdot D(k_x,z=0,\omega-\omega_0). \quad (14)$$

The factor 2 accounts for the superposition of positive and negative frequency side bands.

Formula (13), however, does not have the expression of a 2-D Fourier transform and the computation of the double integral would take too much computer time to be of practical interest. Nevertheless, it can be noted that this double integral can be transformed into a 2-D Fourier transform by applying the change of variables from $\omega$ to $k_z$ defined in (8)

$$\omega = \frac{c}{2}\cdot\sqrt{k_x^2+k_z^2}. \quad (15)$$

This can be written as a function of two new variables $\omega' = \omega-\omega_0$ and $k_z' = k_z - k_{z0}$ as

$$\omega_0+\omega' = \frac{c}{2}\cdot\sqrt{k_x^2+(k_{z0}+k_z')^2}. \quad (16)$$

The following expression of (13) then holds, and can be recognized as a 2-D Fourier transform:

$$d(x,z,t=-t_0) = \frac{1}{(2\pi)^2}\int_{-\omega_s/c}^{+\omega_s/c} dk_z' \int_{k_{x\min}}^{k_{x\max}} \times D'\left(k_x,z=0,\frac{c}{2}\sqrt{k_x^2+(k_{z0}+k_z')^2}-\omega_0\right)\cdot \cdot e^{-jt_0\left((c/2)\sqrt{k_x^2+(k_{z0}+k_z')^2}\right)} \cdot e^{j(k_x x+(k_{z0}+k_z')z)}\cdot\frac{c|(k_{z0}+k_z')|}{2\sqrt{k_x^2+(k_{z0}+k_z')^2}}\cdot dk_x. \quad (17)$$

Furthermore, it is of no use to get all the results from $z=0$ up to a maximum value $z_{\max}$. The radar pulse must travel from the sensor down to the ground to meet the first scatterer; it is useless to search for scatterers at $z$s smaller than $z_0 = ct_0/2$. In order to shift the origin of the $z$ variable to this new value (a necessity when implementing (17) on a computer) the change of variable $z = z_0+\zeta$ must be introduced in (17):

$$d(x,\zeta,t=-t_0) = \frac{1}{(2\pi)^2}\cdot e^{j(k_{z0}\zeta)}\int_{-\omega_s/c}^{+\omega_s/c} dk_z' \int_{k_{x\min}}^{k_{x\max}} \times D'\left(k_x,z=0,\frac{c}{2}\sqrt{k_x^2+(k_{z0}+k_z')^2}-\omega_0\right) \cdot e^{-j\left((ct_0/2)\sqrt{k_x^2+(k_{z0}+k_z')^2}-k_{z0}z_0-k_z'z_0\right)} \cdot\frac{|k_{z0}+k_z'|}{\sqrt{k_x^2+(k_{z0}+k_z')^2}}\cdot e^{j(k_x x+k_z'\zeta)}\, dk_x. \quad (18)$$

The focused data are therefore acquired with the following sequence.

1) 2-D FFT of the range focused data;
2) Change of variables (from $\omega$ to $k_z$ as in (8), the so-called Stolt interpolation);
3) Multiplication times the complex exponential term of (18);
4) Inverse 2-D FFT.

### D. Connection With Conventional Doppler Compression Techniques

So far, we have shown that the focusing process is described exactly by (18). It is interesting to notice that, with the introduction of some approximation, (18) reduces to the conventional Doppler compression technique.

Let us, first, neglect the obliquity factor $|k_z|/\sqrt{(k_x^2+k_z^2)}$ which has little importance due to the small relative bandwidth of SAR signals. Then, since $k_z^2 \gg k_x^2$, let us approximate the square root term $\sqrt{k_x^2+k_z^2}$ with the first two terms of its Taylor series.

The first exponential term inside the double integral of (18) can be approximated as follows:

$$\exp\left[-j\left(\frac{ct_0}{2}\sqrt{k_x^2+(k_{z0}+k_z')^2}-k_{z0}z_0-k_z'z_0\right)\right]\simeq$$
$$=\exp\left[-j\left(\frac{z_0k_x^2}{2(k_{z0}+k_z')}\right)\right]\simeq$$
$$=\exp\left[-j\left(\frac{z_0k_x^2}{2k_{z0}}-\frac{z_0k_x^2k_z'}{2k_{z0}^2}\right)\right] \quad (19)$$

Let us consider again the change of variables

$$\omega'=\frac{c}{2}\cdot\sqrt{k_x^2+(k_{z0}+k_z')^2}-\omega_0 \quad (20)$$

It can be approximated as

$$\omega'=\frac{c}{2}k_z'+\frac{c}{4}\frac{k_x^2}{k_{z0}}-\frac{c}{4}\frac{k_x^2k_z'}{k_{z0}^2}$$

and

$$k_z'\simeq\frac{2}{c}\left[\omega'-\frac{c}{4}\frac{k_x^2}{k_{z0}}\right]\cdot\left[1+\frac{k_x^2}{2k_{z0}^2}\right]$$
$$=\frac{2}{c}\omega'\left[1+\frac{k_x^2}{2k_{z0}^2}\right]-\frac{k_x^2}{2k_{z0}}\left[1+\frac{k_x^2}{2k_{z0}^2}\right]. \quad (21)$$

Furthermore, it can be noted that in practical SAR systems the term $k_x^2/(2k_{z0}^2)$ is always small with respect to 1. However, its effect is not negligible when multiplied times the signal frequency as in the first term of (21). Thus, the following approximation of (21) is adopted

$$k_z'\simeq\frac{2}{c}\omega'\left[1+\frac{k_x^2}{2k_{z0}^2}\right]-\frac{k_x^2}{2k_{z0}}. \quad (22)$$

Eventually, since $k_{z0}=2/c\cdot\omega_0$, (22) can be transformed as follows:

$$k_z'\simeq\frac{2}{c}\omega'+\frac{ck_x^2}{4\omega_0^2}\omega'-\frac{ck_x^2}{4\omega_0}. \quad (23)$$

Eventually, by exploiting (23) and (19), by defining $\tau=2\zeta/c$ and taking into consideration phase and delay components up to the second order, (18) transforms into the following:

$$d(x,\tau,t=-t_0)$$
$$=\frac{1}{(2\pi)^2}\cdot e^{j\omega_0\tau}\int_{-\omega_s/2}^{+\omega_s/2}d\omega'\int_{k_{x\min}}^{k_{x\max}}D'(k_x,z=0,\omega')$$
$$\cdot e^{-j(k_x^2c^2/8\omega_0)(t_0+\tau)}\cdot e^{j(k_x^2c^2/8\omega_0^2)\omega'(t_0+\tau)}$$
$$\cdot\frac{2}{c}\left[1+\frac{c^2k_x^2}{8\omega_0^2}\right]\cdot e^{j(k_xx+\omega'\tau)}dk_x. \quad (24)$$

After these manipulations, it is easy to recognize in (24) that for values of $\tau$ (or $\zeta$ as written above) that are close to zero the change of variables $\omega', k_z'$ has no effects on the focused image. In this case it is easy to recognize the conventional range-Doppler compression technique:

1) the range migration compensation up to the second order (this is done by the second complex exponential term);

2) the compensation of the phase Doppler history (this is done by the first complex exponential term).

On the contrary, when the value of $\tau$ becomes greater and greater (far range) the effect of the Stolt interpolation assumes a fundamental role since (24) shows that it implies the compensation of the parameters variation with range.

### E. Practical Considerations On Focusing Technique

SAR data are two-dimensional and can be organized into a matrix in which, e.g., the sampled returns from the transmission of successive pulses are stored in successive columns. Row and column indices represent, therefore, the slant range and the along-track variables, respectively, (this is the so-called $x-t$ domain).

The compression of the transmitted waveforms can be efficiently performed computing the FFT of each column and multiplying it by the FFT of the reference waveform. Usual care must be paid to the circularity of the resulting convolution. This leaves the data range compressed and the columns FFT transformed ($\omega-x$ domain). The two-dimensional transform of the range focused data $D(k_x,z=0,\omega)$ is finally obtained by FFT transforming the matrix rows. In this $\omega-k_x$ domain the two-dimensional operator expressed by (18) must be applied. The operations to perform are the following.

1) *Change of variable* $\omega\rightarrow k_z$: To transform $D(k_x,z=0,\omega)$ into $D(k_x,z=0,k_z)$ the data values for $\omega'=c/2\cdot\sqrt{k_x^2+k_z^2}-\omega_0$ must be interpolated. The selection of the interpolator is critical for the final image quality and no simple and cheap interpolator will do. However, the very small relative bandwidth of SAR signals reduces the change of variable to a simple shift in the $\omega$ direction, which is a function of $k_x$ only. This shift in the $\omega$ domain can be implemented with no loss of precision if the proper shift operator ($\exp(j\delta_\omega t)$ to shift by $\delta_\omega$) is applied to each row of the data matrix in the time domain, i.e., prior to taking their FFTs. In other words the interpolator is a $k_x,t$ operator that removes the range varying character of the focusing operator.

2) *Multiplication by* $\sqrt{|k_z|/(k_x^2+k_z^2)}$: It is the obliquity factor [7] and, due to the small relative bandwidth of SAR signals, it is almost constant and has, therefore, little importance.

3) *Multiplication by the complex exponential*: This performs the azimuth compression of SAR data using

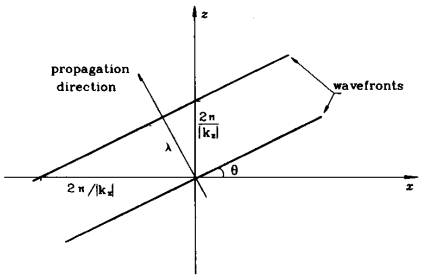


Fig. 3. Geometrical scheme that explains the relationship between wavelength $\lambda$ and wavenumbers $k_x$ and $k_z$ for monochromatic plane wave.

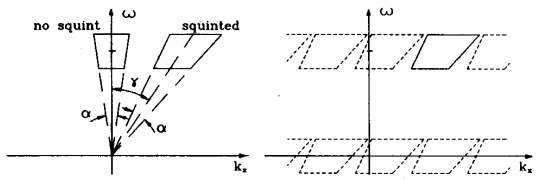


Fig. 4. Frequency-wavenumber data domains for broadside and squinted antenna. (a) Effect of frequency conversion and azimuth sampling of echo data. (b) $\gamma$ is antenna squint angle, $\alpha$ is width of antenna radiation lobe.

the parameters corresponding to the closest approach point.

A final 2-D inverse FFT brings back the data in the $x-z$ domain where modulus detection can be carried out. The multilook techniques, used to reduce speckle noise can be easily implemented: it is enough to partition the matrix of the focused data in the $k_x-k_z$ domain and perform multiple, smaller, inverse FFTs. The images obtained after detection can be added together to improve the signal to noise ratio.

### F. Effect of Antenna Squint

Equation (18) shows that the only parameters whose values must be accurately known to carry out the data focusing are $t_0$ and the velocity of the sensor.

The angle of incidence of a plane wave is uniquely determined by $\omega$ and $k_x$ (see Fig. 3). The width of the antenna radiation pattern identifies an angular sector within the $\omega-k_x$ plane; all plane waves represented by points $(\omega,k_x)$ outside of this sector are rejected by the antenna. Therefore, the data domain is limited in $\omega$ by the bandwidth of the transmitted pulse and in $k_x$ by the constraint due to the antenna radiation pattern. The angular sector rotates if the antenna lobe changes its direction and the data domain changes accordingly (see Fig. 4(a)). Equation (18), however, still retains its full validity and is independent from squint.

This simplicity is somehow obscured by the sampling of the returns at the pulse repetition frequency of the radar. The result of this sampling is the folding in $k_x$ of the signal spectrum as shown in Fig. 4(b). For the processing to be correct, the spectrum must be properly unwrapped and this requires the knowledge of the antenna effective squint, i.e., the angular amount by which the antenna lobe deviates from exact broadside direction. Any uncertainty in the knowledge of the squint angle produces errors: their effect will be unacceptable if the replica of the sampling frequency is missed [12].

Referring to Fig. 4, if $\gamma$ is the squint angle, and $\alpha$ is the antenna beam width, the following relations hold:

$$k_{x\min}=\frac{2\omega_{\min}}{c}\sin\left(\gamma-\frac{\alpha}{2}\right)\quad\text{and}\qquad k_{x\max}=\frac{2\omega_{\max}}{c}\sin\left(\gamma+\frac{\alpha}{2}\right). \tag{25}$$

Equations (25) allow to compute the minimum $f_{\text{prf}}$ necessary to avoid alias, when the transmitted pulse bandwidth and the geometrical parameters of the SAR mission are known. Other constraints on $f_{\text{prf}}$ are equally important and cannot be overlooked, but they are not considered here. The aliased data, as usual, appear as ghosts of the image displaced along the azimuth direction. Due to the sphericity and the rotation of the Earth this alias slightly changes with range.

### G. Effect of the Spherical Spreading

The radiating reflector model and its related approximations are necessary to obtain a migration algorithm which is extremely efficient. The effect of the spherical spreading of the incident radiation can be taken into account rather easily [17]. The Appendix explains how.

## III. MIGRATION IN SPHERICAL GEOMETRY

### A. Travel Times in Spherical Geometry

It is shown in the Appendix that the migration technique of the previous section is effective in providing the solution to the SAR inverse problem when the sensor trajectory is a straight line. Satellite borne sensors do not fit this scheme, and the application of migration techniques in such cases requires a careful analysis.

A rigorous treatment of migration in spherical coordinates is not attempted here. A simpler approach will be followed, that allows to extend the results of the previous section.

Equation (2) shows that, when the sensor trajectory is linear, the measured field can be expressed in terms of the disturbance arrival times. The same concept holds whatever the geometry of the problem. When the sensor flies in a circular orbit over a spherical motionless Earth (see Fig. 5), the travel times, from

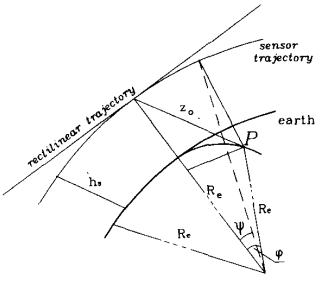


Fig. 5. Geometric layout for sensor flying circular orbit around spherical Earth. Tangent rectilinear trajectory is shown for no sensor antenna squint.

point source to points where the field is sampled, can be expressed as

$$\frac{2}{c}\sqrt{(R_e+h_s)^2+R_e^2-2R_e(R_e+h_s)\cos\varphi\cos\psi} \qquad (26)$$

where $R_e$ is the radius of the Earth, $h_s$ is the altitude of the satellite, and $\varphi$, $\psi$ are, respectively, the elevation angle, with respect to the orbit plane, and the azimuth angle, referred to the direction corresponding to the minimum distance between sensor and point source. The angle $\psi$ spanned by each scatterer is very small (a few degrees), as it depends on the antenna beamwidth and on the system coherent integration time. This allows the expansion of the cosine function into a power series truncated to the quadratic term:

$$\frac{2}{c}\sqrt{(R_e+h_s)^2+R_e^2-2R_e(R_e+h_s)\cos\varphi\left(\cos\psi_0-\psi\sin\psi_0-\frac{\psi^2}{2}\cos\psi_0\right)}$$
$$=\frac{2}{c}\sqrt{z_0^2+2R_e\cos\varphi\sin\psi_0\cdot x+\frac{R_e\cdot\cos\varphi}{R_e+h_s}\cos\psi_0\cdot x^2} \qquad (27)$$

where $x$ is the curvilinear coordinate along the sensor trajectory and $\psi_0$ identifies the position of the point source when it intersects the center of the beam at a distance $z_0$ from the sensor antenna:

$$z_0=\sqrt{(R_e+h_s)^2+R_e^2-2R_e(R_e+h_s)\cos\varphi\cos\psi_0}.$$

Angle $\psi_0$ is zero for no antenna squint, i.e., when the antenna beam points exactly broadside from the sensor path. However, when the radar antenna is squinted, the value of $\psi_0$ changes as a function of the antenna squint and of the source position (i.e., $\varphi$).

If a rectilinear path is considered instead, and it is tangent to the circular orbit where the sensor is located when the center of the beam passes through the source, travel times become

$$\frac{2}{c}\sqrt{z_0^2+2R_e\cos\varphi\sin\psi_0\cdot x_t+x_t^2} \qquad (28)$$

where $x_t$ is now the position along the rectilinear path (the origin being in the point where the two paths are tangent). Equation (28) is just (3) adapted to the geometrical layout of Fig. 5.

Travel times have, therefore, the same functional dependence on the sensor position, both if the true curvilinear path, or the tangent rectilinear one is considered, on condition that the power expansion in (27) is valid. The technique of the previous paragraph applies whenever a rectilinear path can be assumed for the sensor, and it can still be used when the path is curvilinear if the differences between (27) and (28) can be compensated in some way.

Equations (27) and (28) differ only for a factor that multiplies $x$ in the quadratic term. This is enough to forbid exact matching of the proposed migration technique to the circular orbit geometry. However, if squint is moderate and/or integration time is short enough, the resulting aberration of the system is well below the resolution limit posed by the sounding signal bandwidth. If the aforesaid conditions are satisfied, it is possible to approximate (27) as

$$z_0+\frac{2R_e\cos\varphi\sin\psi_0}{z_0}x+\frac{R_e\cos\varphi\cos\psi_0}{(R_e+h_s)z_0}x^2+\cdots \qquad (29)$$

and (28) as

$$z_0+\frac{2R_e\cos\varphi\sin\psi_0}{z_0}x+\frac{x^2}{z_0}+\cdots. \qquad (30)$$

The first term does not change with $x$ and contributes a constant delay. The other terms express the change of the propagation delay with the sensor motion, and are the ones which allow the focusing. The linear term, that produces a shift in $k_x$, is exactly the same in both situations; it is just another way to observe that the antenna squint moves the signal spectrum in the $k_x$ direction. Once the value of the shift in $k_x$ is known, it can be used to correctly evaluate the focusing operator in (18).

The quadratic terms, however, are different and the only way to force the circular orbit case into a

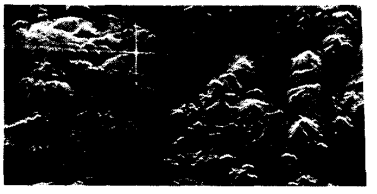

Fig. 6. Example of SAR data focused with proposed technique: Goldstone site is shown (SEASAT data taken in 1978). Dimensions: 25 Km in azimuth (horizontal) by 12 Km in range (vertical). Resolution: 25 m by 25 m (4 looks).

rectilinear path one, is to compress the $x$ scale by a factor $\sqrt{R_e/(R_e+h_s)}\cdot\sqrt{\cos\varphi\cos\psi_0}$. As the sensor position along its trajectory can be expressed as the product of the sensor velocity and time, this amounts to using an "effective" sensor velocity.

The correction factor, however, is range dependent (it changes with $\varphi$). Stated in other words, this means that when the sensor moves along a circular path the hyperbolas generated by point sources have shape variations with range different from the ones that would be experienced with a sensor flying along a straight line.

The quadratic term in (29), however, depends on $z_0$, too. It is possible to modify the value of the scale factor while using a fictitious shift in $z$ (the value of $z_0$ is properly changed), so that the circular path case coincides, at its best, with a linear path one. One possible move is to achieve exact correspondence at two predefined range values, so that the error can be kept very small at all ranges of interest. This procedure allows to compensate the effects of the earth rotation too, as it has been seen on real SEASAT data of the corner reflectors array of Goldstone site where the antenna (see Fig. 6) is located in the middle of the range swath focused simultaneously.

## IV. EXAMPLES OF $\Omega - K$ FOCUSING OF SAR DATA

An example of SAR data focused with the proposed technique of downward continuation or migration, as usually done in seismics, is shown in Fig. 6. The data were taken in 1978 during the SEASAT mission and show the Goldstone site. Four looks have been averaged to reduce speckle; the spatial resolution is about 25 by 25 m. The bright spot clearly visible on the image is the parabolic antenna of Goldstone. Also visible in the upper part of the image is the corner reflectors array.

We said that the quality of the SAR images focused with the proposed $\omega - k$ algorithm is high because of the exact compensation of the data range migration. The experimental evidence of this fact is demonstrated by the comparison of a one look image of the Goldstone area obtained using both a commercially available processor (see the upper part of Fig. 7) and the $\omega - k$ one (see the lower part of Fig. 7). Notice the two azimuth sidelobes (ghost images) near the Goldstone antenna that have been introduced by block correction of the range migration performed by the commercially available processor. The difference between the two results is also visible in the perspective views of the focused Goldstone antenna data shown in Fig. 8, clipped at the same level. Fig. 9 shows also the perspective views of the corner reflectors array as focused with the two techniques.

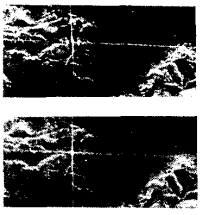

Fig. 7. Upper) Goldstone antenna and the corner reflectors array as focused by a commercially available processor (1 look). Notice ghost azimuth side lobes near antenna. Lower) The same area as focused by the $\omega - k$ processor (1 look). Notice absence of ghost side lobes.

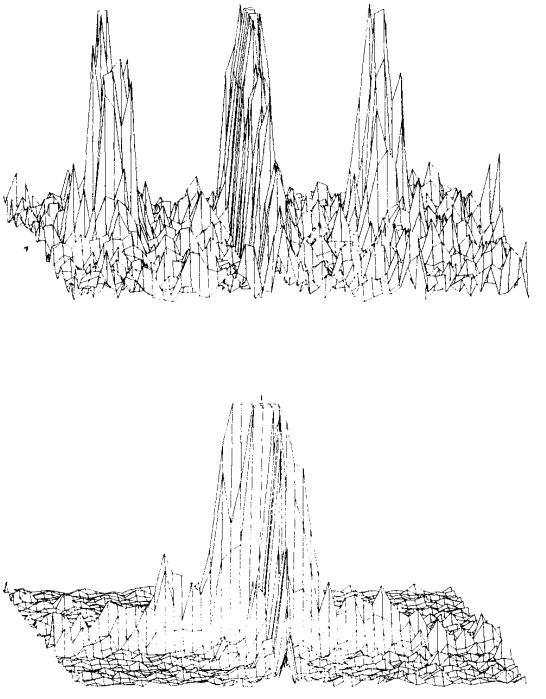

Fig. 8. Perspective views of Goldstone antenna data as processed by commercial processor (upper) and by $\omega - k$ processor (lower).

As a second example, Fig. 10 shows a focused SAR image of the area of Ventura (Los Angeles) taken from the NASA DC-8 airplane (courtesy of Jet Propulsion Laboratory). These data has been focused

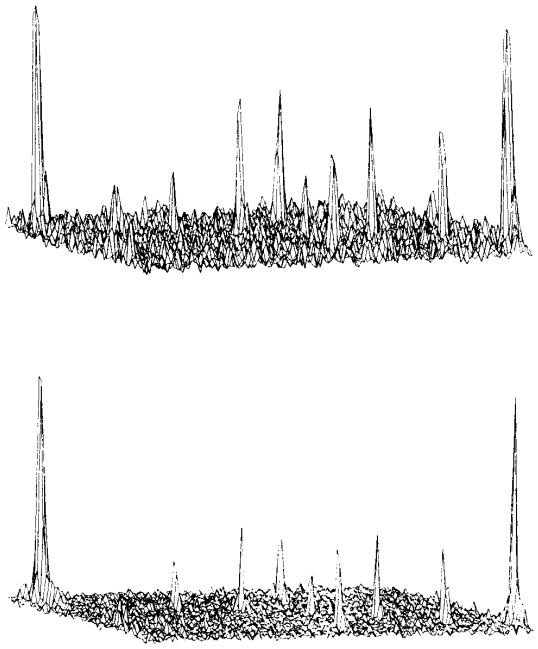

Fig. 9. Perspective views of the corner reflectors array processed by commercial processor (upper) and by $\omega - k$ processor (lower).

Fig. 10. Example of SAR data focused with proposed technique: area of Ventura (Los Angeles) is shown ($L$ band NASA DC-8 data taken in 1988). Dimensions: 3 Km in azimuth (horizontal) by 3 Km in slant range (vertical). Resolution: about 10 m in azimuth by 7 m in slant range (8 : 1 presumming).

with the same software that has been used for the SEASAT data (here the high flexibility) on a PC-AT with 150 lines Fortran-77 code (here the simplicity) in 1 h (here the efficiency).

The effect of the Stolt interpolation of the data is clear by comparing Fig. 10 with Fig. 11 where the same raw data have been focused without the Stolt interpolation. Notice that the near range of the picture (on the top of Fig. 11) is well focused whereas the far range (on the bottom of the picture) shows data that are still to be migrated to take into account the differential phase shift between near range and far range. In other words it is possible to notice the small hyperbola chunks that characterize the migration that still has to be carried out.

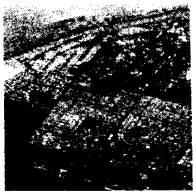

Fig. 11. Same example of Fig. 10. Here the Stolt interpolation has not been used: the near range on the top of the image looks almost completely focused, but the far range shows incomplete focusing.

## V. WHY PROCESSING WITH THE WAVE EQUATION?

All the considerations presented up to now could just be another, maybe futile, exercise in transposition of a concept from the field where it was invented into another field where it perhaps was not needed. However, the huge amount of data that have to be processed in SAR surveys makes it very relevant to study techniques that can reduce the computational burden. The wave equation processing will allow the attainment of the highest resolution without the added costs that today limit the exploitation of full resolution imagery.

Up to now, SAR data have been focused with different techniques which all amount to using filters matched to the diffraction patterns of the point target [13]. The squint of the antenna beam is equivalent to a radial velocity component and can be corrected through a proper relative shifting of data range lines. The problems with this type of processing start when the curvature of the hyperbola cannot be neglected. Then, some sort of frequency-dependent interpolation in the time-wavenumber domain has been attempted but with limited results, at least from the viewpoint of the precision obtainable with limited computational costs [14].

When high resolution was considered necessary, space domain algorithms have been mandatory, with the enormous resulting costs. In fact, the diffraction pattern may well be more than 1000 points long, and each point corresponds to a complex multiplication. The problems increase still as the aperture angle gets larger and larger.

Summarizing, with the classical focusing techniques that have been used up to now for SAR data processing, the hyperbolic traveltime has been approximated with a parabolic phase shift, without attempts to follow precisely the actual time shifts.

Wave equation focusing will allow practically perfect results with minimum cost, i.e., just that of the interpolation in the 2-D Fourier domain. Moreover, it is possible to lump the operations of range migration correction and chirp focusing. An interesting by-product of the proposed method is

that it shows how SAR and seismic data processing are substantially equivalent [6]. Both fields can, therefore, benefit from the possibility of synergy. SAR processing can draw ideas from the pool of sophisticated processing algorithms developed in a field where the cost of careful processing was negligible with respect to the benefits that could ensue. Autofocusing techniques using statistical indicators and residual migration [21] with, e.g., finite difference equations processing could be easily borrowed, if and when the processing precision they can allow could be of any use. Seismic data processing, on the other hand, could greatly benefit from the use of hardware developed for real-time SAR data focusing. In fact seismic data gathering is complex enough to allow for delayed processing. Planned SAR missions will be pouring down a continuous, huge amount of raw data, so that real time focusing will become (and already is) a major research effort.

Another, added feature of frequency domain focusing is the logarithmic dependence of the computing costs upon the radiation wavelength. In fact, for a given resolution, the hyperbola occupies more pixels if the wavelength is increased (same resolution → same antenna size, so that longer wavelength → wider radiation lobe), and the data windows should be made larger. The number of operations, however, increases logarithmically and does not involve real difficulty.

Such decoupling allows the use of lower frequencies (say in the 5-600 MHz range) that means better penetration of the atmosphere, the foliage, and even the Earth surface. Moreover, one might use the same concept to increase the resolution at a given wavelength, rather then using longer wavelengths at a given resolution. Again, a wider antenna beamwidth would be implied and more pixels should be considered in the diffraction pattern.

This extended resolution case is named SPOT SAR [15, 16]. The antenna beam cannot be widened too much without reducing the signal-to-noise ratio by spreading the irradiated energy on too large a surface. Therefore, to increase signal gain, an antenna that is steered so that it points continuously towards the region to be imaged has been proposed. Hence, the name of SPOT SAR.

If frequency domain focusing is used, no big problems appear. However, the alias is now time varying, and should be kept under close control. In fact, the alias depends on the mutual angles between scatterer and satellite, and it increases with the squint of the antenna beam. The limited beamwidth of the antenna can allow the avoiding of confusion, provided that the direction of the antenna is known with sufficient precision at all times.

Finally, we remind another important application: interferometry for digital terrain mapping and for measurement of small terrain motion [22, 23].

## VI. CONCLUSIONS

The technique for SAR data focusing presented in this paper can lead to considerable savings in the sizable computer time needed up to now. In fact only what is needed for quick look focusing, i.e., a cascade of range and azimuth 1-D FFT, two multiplications per sample and two inverse 1-D FFTs are needed for correct focusing. Moreover, the extreme precision of the processing, substantially exact, can lead to higher resolution with lower carrier frequencies. The crossbreeding of seismic and SAR techniques will continue and will be fruitful to both fields.


## ACKNOWLEDGMENTS

The authors wish to express their gratitude to the CSTS of the Italian National Council of Research (CNR) for sponsoring one of the authors (C.P.) during the development of this work, to the European and Italian Space Agencies and to the Italian Ministry of Education.


## APPENDIX. 2D SURVEYS IN 3D SPACE

The scatterers in the SAR situation are 3-D scatterers located on a nonplanar surface. The discussion of Section IIB makes it possible to flatten the scatterers on a conceptual plane, but leaves unaltered the 3-D nature of the direct problem. It is rather simple to show that this fact does not imply relevant changes with respect to the seismic cases.

The radiating reflector approach allows the expression of the field measured by the satellite as [17]:

$$P(x,y,z,\omega) = \frac{j\omega}{4\pi}\iiint s(x',z')\cdot\delta(y')e^{j\omega t_0} \cdot \frac{e^{-j(2\omega/c)\sqrt{(x-x')^2+(y-y')^2+(z-z')^2}}}{\sqrt{(x-x')^2+(y-y')^2+(z-z')^2}}\,dx'\,dy'\,dz' \tag{31}$$

where $x$, $z$ are the axes in the plane defined by the orbit. In this section we take that as a straight line. The scatterers are described by a distribution of sources $s(x,z)$ lying on the $x-z$ plane, all emitting at time $t=0$. The third coordinate $y$, is orthogonal to this plane. Scalar wave equation is used [18].

If we could measure the data for all $y$s, we could Fourier transform, and for $k_y = 0$ we would get

$$P(x,k_y,z,\omega) = -j\omega\frac{\pi}{2}\iint s(x',z')e^{j\omega t_0}H_0^{(2)} \times\left(\sqrt{4\frac{\omega^2}{c^2}-k_y^2}\cdot\sqrt{(x-x')^2+(z-z')^2}\right)dx'\,dz' \tag{32}$$

$$P(x,k_y=0,z=0,\omega)$$
$$=-j\omega\frac{\pi}{2}\iint s(x',z')e^{j\omega t_0}H_0^{(2)}$$
$$\times\left(\frac{2\omega}{c}\sqrt{(x-x')^2+z'^2}\right)dx'\,dz' \tag{33}$$

$$P(k_x,k_y=0,z=0,\omega)$$
$$=\frac{\omega}{2}\iint s(x',z')e^{j\omega t_0}\frac{\exp\left(-jz'\sqrt{4\frac{\omega^2}{c^2}-k_x^2}\right)}{\sqrt{4\frac{\omega^2}{c^2}-k_x^2}}$$
$$\cdot e^{-jk_x x'}\,dx'\,dz'. \tag{34}$$

Using the change of variables (8) we would then get the migrated data [19]. However, we only measure $P(x,y=0,z=0,\omega)$ while we need $P(x,y,z=0,\omega)$. We also have [20] that

$$P(k_x,y=0,z=0,\omega)=-j\omega\frac{\pi}{2}\iint s(x',z')e^{j\omega t_0}H_0^{(2)}$$
$$\times\left(z'\sqrt{4\frac{\omega^2}{c^2}-k_x^2}\right)e^{-jk_x x'}\,dx'\,dz'. \tag{35}$$

If we approximate the Hankel function with its expansion for high values of the argument (and they are high indeed, since they might be of the order of several millions), we get

$$P(k_x,y=0,z=0,\omega)$$
$$\simeq\omega\sqrt{\frac{\pi}{2}}e^{-j\pi/4}\iint s(x',z')e^{j\omega t_0}$$
$$\cdot\frac{\exp\left(-jz'\sqrt{4\frac{\omega^2}{c^2}-k_x^2}\right)}{\sqrt{z'}\sqrt[4]{4\frac{\omega^2}{c^2}-k_x^2}}e^{-jk_x x'}\,dx'\,dz'. \tag{36}$$

Change of variable (8) now produces the final equation, in a slightly different form than in (17):

$$\frac{s(x,z)}{\sqrt{z}}=e^{j\pi/4}\sqrt{\frac{2}{\pi}}\iint P\left(k_x,y=0,z=0,\frac{c}{2}\sqrt{k_x^2+k_z^2}\right)$$
$$\cdot e^{-j(t_0c/2)\sqrt{k_x^2+k_z^2}}\sqrt{\frac{|k_z|}{k_x^2+k_z^2}}e^{j(k_x x+k_z z)}\,dk_x\,dk_z \tag{37}$$

REFERENCES


[1] Elachi, C., et al. (1986)
SIR-B The second shuttle imaging radar experiment.
*IEEE Transactions on Geoscience and Remote Sensing*, **GE-24**, 4 (1986), 445–452.

[2] Fitch, J. P. (1988)
*Synthetic Aperture Radar*.
New York: Springer-Verlag, 1988.

[3] Wehner, D. R. (1987)
*High Resolution Radar*.
Nordwood, MA: Artech House, 1987.

[4] Ausherman, D. A., Kozma, A., Walker, J. L., Jones, H. M., and Poggio, E. C. (1984)
Developments in radar imaging.
*IEEE Transactions on Aerospace and Electronic Systems*, **AES-20** (July 1984), 363–398.

[5] Munson, D. C. (1987)
An introduction to strip–map synthetic aperture radar.
In *Proceedings of the International Conference on Acoustics, Speech, and Signal Processing*, 1987, 2245–2248.

[6] Bolondi, G., Rocca, F., and Savelli, S. (1978)
A frequency domain approach to two-dimensional migration.
*Geophysical Prospecting*, **26**, 4 (Dec. 1978), 750–772.

[7] Claerbout, J. F. (1985)
*Imaging the Earth Interior*.
Oxford: Blackwell Scientific Publications, 1985.

[8] Gazdag, J., and Sguazzero, P. (1984)
Migration of seismic data.
*Proceedings of IEEE*, **10** (Oct. 1984), 1302–1315.

[9] Dragoset, W. H. (1988)
Marine vibrators and the Doppler effect.
*Geophysics*, **53**, 11 (Nov. 1988), 1388-1398.

[10] Elachi, C., Roth, L. E., and Scaber, G. C. (1984)
Spaceborne radar subsurface imaging in hyperarid regions.
*IEEE Transactions on Geoscience and Remote Sensing*, **GE-22** (1984), 382–387.

[11] Cafforio, C., Prati, C., and Rocca, F. (1989)
SAR real time on board processing: the polyphase algorithm.
*Signal Processing*, **18**, 4 (Dec. 1989), 397–411.

[12] Li, F., Held, D., Curlander, J. C., and Wu, C. (1984)
Doppler parameter estimation from spaceborne synthetic aperture radar.
*IEEE Transactions on Geoscience and Remote Sensing*, **GE-22**, 2 (1984).

[13] Curlander, J. C. (1986)
Performances of the SIR-B digital image processing subsystem.
*IEEE Transactions on Geoscience and Remote Sensing*, **GE-24**, 4 (1986), 649–652.

[14] Wu, K. H. (1985)
Extensions to the step transform to accommodate nonlinear range migration and high squint angle.
*IEEE Transactions on Aerospace and Electronic Systems*, **25** (May 1985), 338–344.

[15] Prati, C., Monti Guarnieri, A., and Rocca, F. (1991)
Spot mode SAR focusing with the $\omega-k$ technique.
*Proceedings of IGARSS'91*, Helsinki, June 1991.

[16] Prati, C., Rocca, F., Kost, Y., and Damonti, E. (1991)
SIR-C/X-SAR: the estimation of the Doppler centroid ambiguity.
*Proceedings of IGARSS'91*, Helsinki, June 1991.

[17] Cheng, G., and Cohen, S. (1984)
The relationship between Born inversion and migration for common-midpoint stacked data.
*Geophysics*, **49** (Dec. 1984), 2117–2131.

[18] Ulaby, F. T., Moore, R. K., Fung, A. K. (1986)
*Microwave Remote Sensing—Active and Passive*, Vol. III.
Nordwood, MA: Artech House, 1986.

[19] Stolt, R. (1978)
Migration by Fourier transform.
*Geophysics*, **43**, 1 (1978), 23–48.

[20] Schneider, W. A. (1978)
Integral formulation for migration in two and three dimensions.
*Geophysics*, **43**, 1 (1978), 49–76.

[21] Cafforio, C., Prati, C., and Rocca, F. (1991)
Full resolution focusing of SEASAT SAR images in the frequency-wave number domain.
*International Journal of Remote Sensing*.

[22] Prati, C., and Rocca, F. (1991)
Limits to the resolution of elevation maps from stereo SAR images.
*Int. Journal of Remote Sensing*, **11**, 12, 2215–2235.

[23] Prati, C., Rocca, F., Monti Guarnieri, A., and Damonti, E. (1990)
Seismic migration for SAR focusing: Interferometrical applications.
*IEEE Transactions on Geoscience and Remote Sensing*, **28**, 4 (July 1990), 627–640.

**Ciro Cafforio** graduated from the Politecnico di Milano, Italy, in 1973.

In 1973 he joined the Electronic Department of the Politecnico di Milano, where eventually he became Associate Professor of Radiotechniques. Since 1988 he has been with the Dipartimento di Elettrotecnica ed Elettronica of the University of Bari, Italy. His research interests include signal processing, television coding and synthetic aperture radar signal processing.

Mr. Cafforio is a member of the Italian Electrotechnical and Electronic Association.

**Claudio Prati** was born in Milan, Italy, on Mar. 20, 1958. He received the "laurea" in electronic engineering in 1983, and the Ph.D. degree in 1987, both from the Politecnico di Milano.

In 1987 he joined the Centro Studi Telecommunicazioni Spaziali of the National Research Council in Milan. He visited the Department of Geophysics of Stanford University as Visiting Scholar during the autumn quarter of 1987. His main research interests concern digital signal processing in noise suppression. He has studied and tested speech enhancement techniques for mobile radio communication. In emission tomography, he has studied the tissue absorption problem, and in synthetic aperture radar, he has studied new focusing techniques and interferometrical applications of synthetic aperture radar data.

**Fabio Rocca** graduated in electronic engineering from the Politecnico di Milano in 1962.

He has worked in the Department of Electronic Engineering at the Politecnico, where he is now Professor of digital signal processing. He visited the System Sciences Department of UCLA during 1967–1968, and then the Department of Geophysics of Stanford University as Visiting Professor in 1978, 1979, 1981, 1983, 1986, and 1987–1988. He is currently Coordinator of the EEC research program in geosciences.

Dr. Rocca is Past President of the European Association of Exploration Geophysics and is an honorary member of the Society of Exploration Geophysics.